J Intell Robot Syst (2014) 74:173–191
DOI 10.1007/s10846-013-9987-3

A Novel Actuation Concept for a Multi Rotor UAV

Pau Segui-Gasco · Yazan Al-Rihani · Hyo-Sang Shin · Al Savvaris

Received: 1 September 2013 / Accepted: 30 September 2013 / Published online: 22 November 2013

Abstract This paper proposes a novel strategy to improve the performance and fault tolerance of multi-rotor vehicles. The proposed strategy uses dual axis tilting propellers and thus enables three different actuation mechanisms, namely, gyroscopic torques, thrust vectoring and differential thrusting. Unlike the conventional quadrotor, the proposed strategy offers a wider range of control torques by combining the three actuation mechanisms. Conventional quadrotors cannot be reconfigured if one of rotors fails. However, the proposed strategy is still able to reconfigure the vehicle with complete failure of one rotor and a pair of adverse motors. In order to prove this concept, a dual axis tilting UAV is first designed and prototyped. Next, a mathematical representation of the prototyped vehicle is modelled and verified using experiments. Then, a control system is developed based on a PD controller and pseudoinverse control allocator and validated through tests on a rig and flight tests. The tests show that the vehicle is faster than a conventional counterpart and that it can resist the failure of two rotors. Finally, this paper suggests how to lead further substantial improvements in performance.

Keywords Multi-rotor vehicle · Agility and reliability · Actuation mechanism · Gyroscopic torques · Thrust vectoring · Differential thrusting · Control allocation

P. Segui-Gasco · H.-S. Shin (✉) · A. Savvaris
Departament of Engineering Physics,
Cranfield University, Cranfield MK43 0HT, UK
e-mail: h.shin@cranfield.ac.uk

P. Segui-Gasco
e-mail: p.seguigasco@cranfield.ac.uk

Y. Al-Rihani
King Abdullah Design an Development Bureau
(KADDB), Amman, Jordan
e-mail: yazan.rihani@kaddb.mil.jo

1 Introduction

In recent years inexpensive lightweight Unmanned Aerial Vehicles (UAV) have proliferated vastly as an alternative to more expensive and complex manned systems. The operational experience of small UAVs has proven that their technology can bring a dramatic impact to both military and civil arenas. This includes, but not limited to: obtaining real-time, relevant situational awareness before making contact; helping commanders to lead appropriate decision making; and reducing risk to the mission and operation. In R&D many prototype technologies, algorithms and techniques are tested in the, now ubiquitous, quadrotor platform. Quadrotors have become very popular due to their simplicity, ease of use and maintenance, and low cost.

For real applications, quadrotors may become larger because they might need to carry more payloads and/or should be resilient to external disturbances such as a wind gust or turbulence. When one tries to scale them up, agility and reliability become an important issue. As a multirotor vehicle scales up there are two main problems that slow down its dynamic response, i.e., decrease agility of the vehicle. First, as stated by [11], if the vehicle scales up, its inertia builds up and consequently it demands much larger control moments to create the same angular acceleration on the airframe. Second, as the weight increases, assuming a constant disc loading, the propeller size increases and hence its inertia. Note that the torque required for an equivalent angular acceleration of the propeller, and hence that of the vehicle, scales with the square of the vehicle's weight. However, the motor torques are constrained by the maximum amperage of the motors which is physically limited. Therefore, as the vehicle's weight increases, the range of attainable angular accelerations is reduced, and consequently the control bandwidth of the vehicle decreases. These are physical boundaries that the conventional quadrotor has in its performance. If quadrotors are operated in mission environments where they might require aggressive and fast manoeuvres, for example complex urban environments, the agility issue could become important.

In the conventional quadrotor, if any of the actuators fails, the vehicle is completely destabilised because its inherent dependence on the symmetry of the lift. In order to mitigate this reliability issue, two approaches were proposed in our previous study [10]: the first approach uses propellers with a variable pitch and the second approach shifts the CG. Although both of the proposed approaches could reconfigure the controllability in pitch and roll axes, the yaw axis remains uncontrollable. Hence, the two main issues for a large quadrotor platform are fault tolerance and agility: When an arm fails, the vehicle is completely uncontrollable; and the control bandwidth of the system dramatically decreases as the weight increases.

There have been some attempts to overcome these issues. One naive approach is to increase the number of rotors. Typical examples include six rotors, called hexarotors, or eight, named octorotors. This approach has several advantages, among those are mechanical simplicity and its increased number of actuators and hence, its reliability. However, this approach might fail to increase the bandwidth, because the increase in the number of propellers must match that in weight to keep the weight carried by each propeller constant. In this case, radius and inertia of each propeller should be kept low to maintain the bandwidth high. However, this could imply a possibly unacceptable large number of propellers for moderate weights. As a consequence of the number of arms, for the same payload, they would increase the fraction of the structural weight, increasing the inertia, and hence reducing the bandwidth.

Rather than adding more rotors, other approaches involve a variety of actuation devices. As usual with aircraft design, key aspects that must be considered are its size and weight. A very effective approach has been shown by Cutler et al. [4] using propellers with variable pitch. In their approach, while the authors manage to keep the weight down, they increase the bandwidth of its actuators by almost an order of magnitude. However, the reliability is still an issue, because a failure of an actuator might result in instability. In [9], Control Moment Gyroscopes (CMG) are proposed to increase the bandwidth of the actuators of the control system merging a thrust vectoring approach with additional flywheels to use as CMG and a vane system for thrust vectoring. This approach, however, greatly complicates the system and could significantly increase its weight because the aircraft needs to carry the extra weight of the flywheels and the thrust vectoring vane system. Gress [6] came up with the idea of using Opposed Lateral Tilting (OLT) as a means of using the gyroscopic effects for governing the pitch attitude of aircraft, using the propellers as gyroscopes. In his latest work [7], OLT is proved to give higher control authority than other means of actuation such as vaned fans. Also, this concept has been explored by [8], where the authors provide evidence of the effectivity of this technique in simulation. In [1] these concepts are put into practice with the vehicle T-Phoenix UAV, providing a detailed model and a control strategy for hovering, showing experimental evidence of the feasibility of the

OLT strategy. In another work [12] the authors provide also a survey of OLT technology and a more in depth modelling of the tilting phenomena.

The aim of this paper is to find a novel actuation architecture that overcomes the two major problems with the convectional quadrotors: control bandwidth and fault tolerance. Conventional multi-rotors use differential thrusting; most of tilt rotor vehicles use thrust vectoring; and some other vehicles utilise the gyroscopic torques in [7, 9]. The key idea of the proposed concept is to integrate all these three actuation modes into one system. This approach is similar to [9], but in a simpler and more integrated way. Instead of introducing extra devices to use as flywheels and vanes, the propellers of the vehicle are used as flywheels themselves by introducing dual axis tilting to the propellers. This concept enables exploitation of the three different actuation types. Gyroscopic torques are achieved by using the angular momentum and fast tilting of its rotational axes. Thrust vectoring is achieved by orienting the thrust of each propeller independently of the body. Differential thrusting is obtained by the conventional quadrotor strategy of differential angular velocities in the rotors.

In order to prove that the proposed concept is actually able to improve reliability and agility, a new multi-rotor arm concept is developed. Then, a quadrotor UAV, which uses this arm concept to generate the three actuation mechanisms, is also designed and prototyped. A high fidelity simulation model of the novel quadrotor is also developed to assist the understanding of its dynamics and design a control system. Then, a control system is designed based on the classical control theory and pseudoinverse control allocation. Furthermore, a fault tolerant control is developed by modifying the control effectiveness matrix. The performance of the proposed concept and all designed controllers is validated through simulation, experiment on a test rig, and flight test. Analysis and discussion of the results focus on verifying wether the new control system actually increases the bandwidth and degree of fault tolerance.

The paper layout is as follows: first the design and prototyping of the quadrotor are presented. Second, an overview of the simulation model is described. Next, the design of the control system is detailed. Then, the tests performed are described. Finally, an analysis and discussion of the results are presented.

2 Prototyping

A realisation of this novel arm concept is shown in Fig. 1a. Here we have used commercially available parts to minimise the number of custom manufactured parts. This design is based around the servoblock [13] part which serves as a frame to mount a standard size RC servo which allows it to move the whole arm around its axis. In the arm there is mounted another servo which is connected through a pushpull mechanism to the motor mount which swivels parallel to the servo lever. Thus, the propeller rotational axis can be freely configured with the two angles generated by

(a) Novel arm prototype

(b) Vehicle prototype

Fig. 1 Arm 3D model and built prototype

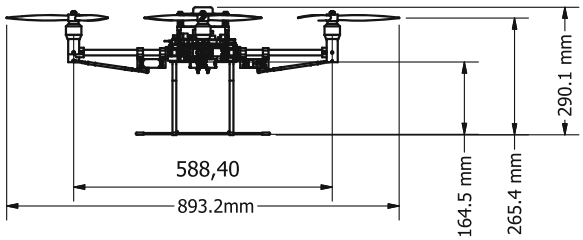

Fig. 2 Platform technical drawing

the servomotors. Henceforth, the naming of these two angles/motions will be named push-pull and servoblock.

The vehicle prototype can be seen in Fig. 1b. The nominal weight of the vehicle is three kilograms and its dimensions are illustrated in Fig. 2. All selected and designed components and their weights are represented in Table 1. The servomotors used at the servoblock and pushpull are the HS-7940TH by Hitec. The propellers are three bladed because of the even distribution of its mass and inertia, and the model is the master airscrew 3 blade 12 × 6 in. The motors used are the brushless DC outrunners MK3638 by Mikrokopter. The ESC used were the Roxxy Bl Control 930-6 from Robbe. The vehicle had two batteries, one to power the servomotors, a LiPo 7.4 V 2S1P 3200 mAh 25 C and another one to power the motors, a LiPo 14.8 V 4S1P 5000 mAh 20 C. The sensor suite used was an IMU by SBG systems, the IG-500N, this unit has an embedded processor able to output filtered attitude and position data up to a 100 Hz. All the control software was run on a Max32 board by Digilent, that runs a PIC32, and the servomotors and ESCs were driven by a Parallax Propeller board. The telemetry was implemented using XBee modules by Digi.

A more detailed overview of the vehicle design can be found in the Theses by Al-Rihani [2] and Segui-Gasco [5] or in the paper by the authors [3]. Note that, whereas [3] focuses on design and modelling of the proposed vehicle, this paper focuses more on control system design and proof on on the entire concept.

Table 1 Breackdown of components and their weights

Component	Weight (g)
IMU(SBG IG-500N)	44
IMU voltage level converter	10
Flight Computer (chipKIT Max32)	36
Servo controller	19
GPS antenna	38
Wireless (xbee pro)	2
Xbee explorer regulated	2
BATTERY (LiPo 14,8 V 5350 mAh)	504
BATTERY (LiPo 7.4 V 3200 mAh)	185
RC receiver(Spectrum)	5
Harnesses and connectors	243
4x Motor with adapter(MK3638)	4 × 125
4x Propeller (3-blade 12 × 6)	4 × 45
4x ESC (Roxxy BL 930-6)	4 × 32
4x Motor holding bracket	4 × 14
4x servoblock	4 × 25
8x servo (HS-7940TH)	8 × 66
4x Adapters and holders	4 × 30
4x Aluminum Arm	4 × 15
8x Clamping hub	8 × 9
4x Push Pull arm	4 × 9
4x Arm tip mount	4 × 5
2x Center plate	2 × 100
Landing gear	55
Battery holder	41
Total	3057

3 Modelling

In this section a general overview of the main phenomena involved in the modelling of the actuation system is described. This can be found with further elaboration on the paper by the authors [3] which is specifically focused on the modelling and simulation of the vehicle. The modelling of the actuation phenomena has 3 main parts. One is the development of the rigid body relations of the tilting propeller that describe the torque as a function of the vehicle motion and the tilting motions. Another one is the characterisation of the propellers in terms of thrust and torque coefficients, and finally the individual actuators that create the tilting motion, servomotors, and the motors that vary the propeller's angular speed are dynamically characterised.

3.1 Gyroscopic Actuation Modelling

The gyroscopic effects are modelled as the reactions generated by individual rotors spinning due

to the vehicle motion and tilt motion of the actuators. In other words, it is assumed that each of the rotor-propeller assembly, shown in Fig. 3a, does the job of a flywheel that, and when tilted, creates the gyroscopic reaction torques. The relations between the motion of the rotor j and the moments applied onto it expressed on the reference frame i are given by the Euler equation:

$$ {}^{i}\mathbf{M}_j = {}^{i}\mathbf{I}_j {}^{i}\boldsymbol{\alpha}_j + {}^{i}\boldsymbol{\omega}_j \times {}^{i}\mathbf{I}_j {}^{i}\boldsymbol{\omega}_j \tag{1} $$

where ${}^{i}\mathbf{M}_j$ is the moment in the centre of gravity of the rotor in arm j expressed in reference frame i, see Fig. 3b, ${}^{i}\mathbf{I}_j$ is the inertia tensor about the CG in the reference frame i, ${}^{i}\boldsymbol{\omega}_j$ is the total angular velocity of the body j and ${}^{i}\boldsymbol{\alpha}_j$ is the total angular acceleration of the body j in the reference frame i ,i.e. ${}^{i}\boldsymbol{\alpha}_j = \frac{\mathrm{d}}{\mathrm{d}t}{}^{i}\boldsymbol{\omega}_j$.

As can be inferred from Fig. 3b, the vehicle presents symmetry both around the x-z plane and the y-z plane. Hence, the development of the equations is the same for all four arms if the reference frame is adequately transformed. For this reason, here only the equations with respect to arm 3 will be developed and then, the equations regarding the remaining arms can be obtained by an appropriate frame change. Arm 3 will be referred to, herein, as Standard Arm or Arm 3 indifferently.

With the nomenclature stablished in Fig. 4, the angular velocity of the of rotor in arm 3, expressed

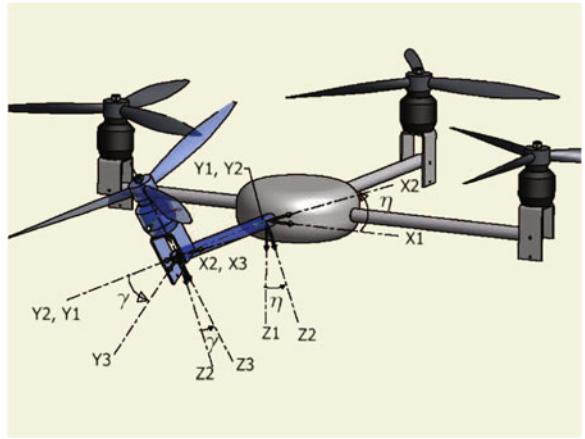

Fig. 4 Reference frames used in the development

in terms of reference attached to the motor stator (frame 3), will be given by:

$$ {}^{3}\boldsymbol{\omega} = \underbrace{{}^{3}\mathbf{i}_1 p + {}^{3}\mathbf{j}_1 q + {}^{3}\mathbf{k}_1 r}_{\text{Vehicle Motion}} + \underbrace{{}^{3}\mathbf{j}_1 \dot{\eta}}_{\text{servoblock}} + \underbrace{{}^{3}\mathbf{i}_2 \dot{\gamma}}_{\text{push pull}} + \underbrace{{}^{3}\mathbf{k}_3 \Omega}_{\text{Motor}} \tag{2} $$

where the vectors ${}^{i}\mathbf{i}_j\ {}^{i}\mathbf{j}_j\ {}^{i}\mathbf{k}_j$ represent the unit vectors of reference frame j expressed in terms of the reference frame i, see Fig. 4 where the reference frames are detailed. The angular acceleration is the derivative of the angular velocity, hence:

$$ {}^{3}\boldsymbol{\alpha} = \frac{\mathrm{d}^3\boldsymbol{\omega}}{\mathrm{d}t} \tag{3} $$

The inertia tensor of the rotor, Fig. 3a, is symmetric because of the use of 3-blade propellers,

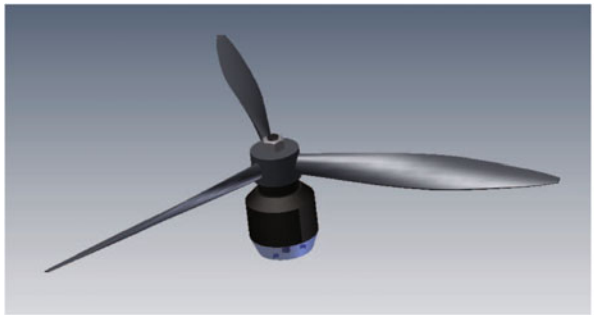

(a) Spinning Body, motor estator + propeller

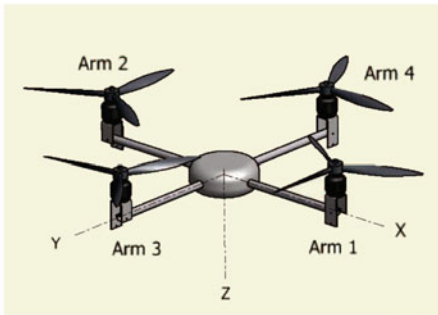

(b) Arm numbering

Fig. 3 Spinning body and arm numbering illustration

hence, it does not change with respect of its rotation axis. The reference frame 3 is coincident with the principal inertia axes of the rotor, and so the inertia tensor is constant around those axes and given by:

$$^3\mathbf{I} = \begin{bmatrix} I_{xx} & 0 & 0 \\ 0 & I_{yy} & 0 \\ 0 & 0 & I_{zz} \end{bmatrix} \tag{4}$$

Thus, the moments can be calculated with the Euler equation around the reference frame 3:

$$^3\mathbf{M} = {}^3\mathbf{I}^3\boldsymbol{\alpha} + {}^3\boldsymbol{\omega} \times {}^3\mathbf{I}^3\boldsymbol{\omega} \tag{5}$$

Since the interest is the actions that the spinning assembly exerts onto the airframe the reactions shall be calculated and, also, for convenience are expressed into the vehicle frame, i.e. reference frame 1. Therefore, introducing and simplifying all the expressions above, the moments that the spinning body applies onto the airframe in the reference frame of the vehicle, $^1\mathbf{M}_{\text{Gyro}}$, are given by:

$$^1\mathbf{M}_{\text{Gyro}} = \mathbf{R}_{3\text{to}1}(-{}^3\mathbf{M}) = \begin{bmatrix} {}^1\mathbf{M}_{\text{Gyro}_X} \\ {}^1\mathbf{M}_{\text{Gyro}_Y} \\ {}^1\mathbf{M}_{\text{Gyro}_Z} \end{bmatrix} \tag{6}$$

where, $^1\mathbf{M}_{\text{Gyro}_X}$, $^1\mathbf{M}_{\text{Gyro}_Y}$ and $^1\mathbf{M}_{\text{Gyro}_Z}$ are the scalar moments in each axis which are specified on the Appendix.

Now, taking advantage of the vehicle symmetry these equations can be transformed to express the action of any other of the vehicle arms by switching the axes and maintaining the sign criteria in Fig. 4. This is done by adding up each individual arm:

$$^1\mathbf{M}_{\text{Gyro}_j} = \mathbf{R}_{3\text{to}j}{}^1\mathbf{M}_{\text{Gyro}} \tag{7}$$

where $\mathbf{R}_{3\text{to}j}$ represent the transform matrix from arm 3 to the arm j, obviously, because the equations have been developed in arm 3, $\mathbf{R}_{3\text{to}3}$ is the identity. Thus, the total action exerted by the four different arms will be:

$$\mathbf{M}_{\text{Gyro}_{\text{Total}}} = \sum_{j=1}^{4} {}^1\mathbf{M}_{\text{Gyro}_j} \tag{8}$$

3.2 Thruster Characterisation

The thrust generated by the propellers is modelled by means of constant thrust coefficient given by:

$$T = \rho A(\Omega R)^2 C_T \text{ and } Q = \rho A(\Omega R)^2 R C_Q \tag{9}$$

Experimentally the coefficients were found to be: $C_T = 0.013$ and $C_Q = 0.0013$.

3.3 Component System Identification

Another vital part of the model is to find the dynamics of the motors and the servomotors because they determine, respectively, the rate of change of thrust and the time derivatives of the tilt angles which create the gyroscopic torques. A series of experiments were carried out yielding the following transfer functions for each actuator.

$$G_{\text{Motor}} = \frac{\Delta\omega\ (\frac{\text{rad}}{s})}{\Delta\tau\ (0 \text{ to } 1)} = \frac{e^{-0.035s}9.19}{(1 + 0.16s)} \tag{10}$$

$$\begin{aligned} G_{\text{servoblock}} &= \frac{\eta\ (\text{rad})}{\eta_{\text{Requested}}\ (\text{rad})} \\ &= \frac{1228.05}{1228.05 + 49.18s + s^2} \end{aligned} \tag{11}$$

$$\begin{aligned} G_{\text{pushpull}} &= \frac{\gamma\ (\text{rad})}{\gamma_{\text{Requested}}\ (\text{rad})} \\ &= \frac{1212.73}{1212.73 + 51.11s + s^2} \end{aligned} \tag{12}$$

3.4 Thrusting Torques

The thrusters create two main sources of aerodynamic torques. One is the torque created by the thrust and the other is the drag torque. Again for arm 3 they can be expressed as:

$$\begin{aligned} \mathbf{M}_{\text{Motor}_3} &= \mathbf{r}_{\text{Hub2CG}} \times \mathbf{T}_{\text{Motor}} + \mathbf{Q} \\ &= T \begin{bmatrix} l\cos(\gamma)\cos(\eta) - H\sin(\gamma) \\ -H\cos(\gamma)\sin(\eta) \\ -l\cos(\gamma)\sin(\eta) \end{bmatrix} \\ &\quad \pm Q \begin{bmatrix} \cos(\gamma)\sin(\eta) \\ -\sin(\gamma) \\ \cos(\gamma)\cos(\eta) \end{bmatrix} \end{aligned} \tag{13}$$

where H and l are the vertical and lateral separation of the CG and the propeller hub respectively. For the remaining arms the torque is easily calculated again by projection as done in Eq. 7 and, hence, the total aerodynamic moment on the vehicle is:

$$\mathbf{M}_{\text{Motor}_{\text{Total}}} = \sum_{j=1}^{4} \mathbf{R}_{3\text{to}j}\mathbf{M}_{\text{Motor}_3} \tag{14}$$

4 Control System Design

The vehicle, by its nature, is open loop unstable, so a control system should be properly designed. The general structure and architecture of the control system is shown in Figs. 5 and 6. The control system is based on two main components, the control law and the control allocator. The control law is a stability augmentation system that receives the pilot commands from the transmitter and the motion information from the IMU sensor and issues the required rolling, pitching yawing moments and thrust. The design of the control system is based on the conventional control theory, especially a PD controller because it is desired to have a control system which is simple to tune and efficient to implement so as to take best advantage of our sophisticated over-actuated system. The architecture chosen was a PD-like loop for each axes and a control allocator, see Fig. 6. The designed control allocator, receives the rolling, pitching yawing moments and thrust and distribute them among the 12 actuators. This enables to utilise several known advantages, among others: allowance to accommodate actuator failures and capability to choose the actuator combination to optimise some cost function, e.g. minimising drag, deflection or energy consumed. The Weighted Pseudorinverse method presents these numerous advantages, besides its simplicity. For this reason, this method is selected as the control allocator in this study and will be detailed in the following section.

4.1 Control Allocation

Actuator Model Linearisation The first step to design a proper control allocator is to understand the control effectiveness results from the proposed control actuations. Therefore, the control effectiveness matrix, B, must be found such that:

$$\mathbf{v} = [M,\ N,\ L,\ T]^T = h(t, \mathbf{x}, \mathbf{u}) \approx B\mathbf{u} \tag{15}$$

where $t \geq 0$ is time, $\mathbf{x} \in \mathbb{R}^r$ is the state vector, $\mathbf{u} \in \mathbb{R}^m$ is the physical actuators input vector and $\mathbf{v} \in \mathbb{R}^n$. The function h in the above equation is a nonlinear function of the time, t, the state vector, $\mathbf{x}$, and the physical control inputs $\mathbf{u}$ that maps the effects of the physical control inputs and the vehicle motion to the Roll (M), Pitch (N), Yaw (L) moments and thrust (T) domains. Note that the mathematical model and PD controller are based on roll, pitch and yaw moments and thrust domains as in the conventional modelling and control approaches for aircraft.

To carry out this linearisation some assumptions were taken. Around the trim point the thrust and torque generated by the propellers is assumed to be linear and proportional to the actuator commands. This is a realistic assumption because the commands to the motors are issued to the ESC in terms of PWM uptime which is linear with the thrust, rather than in terms of angular speed. The

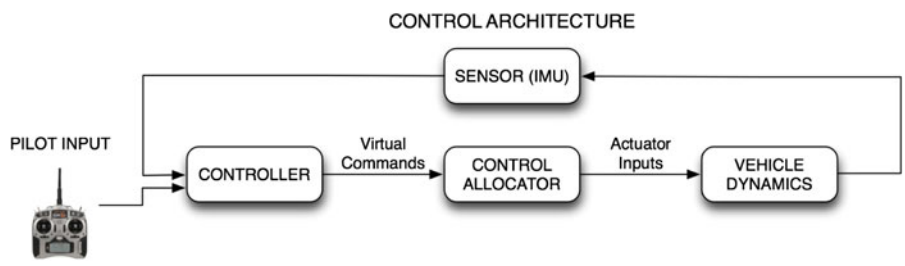

Fig. 5 Main structure of the control system

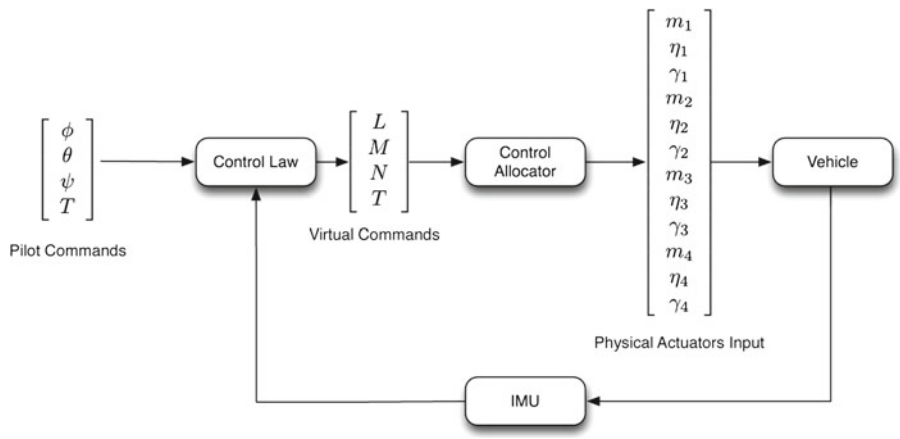

Fig. 6 Architecture of the control system

proportionality constants are defined herein as μ for the thrust and κ for the torque. Also, another simplification is that the deflection angles η and γ are sufficiently small so that $\sin(\gamma) \approx \gamma$, $\sin(\eta) \approx \eta$, $\cos(\gamma) \approx 1$ and $\cos(\eta) \approx 1$. This is reasonable given that the maximum deflection of the servos is constrained by the arm clearance and is around 10°. Finally, another further simplification, is that the rate of change of the servomotor angle is equal to the average rate of change over the rise part of the response. That is, the commanded angle divided by the rise time, $\dot{\eta} \approx \frac{\eta}{t_r}$ and $\dot{\gamma} \approx \frac{\gamma}{t_r}$.

All these is put together to form the control effectiveness matrix for the standard arm, (arm 3), with a column for each individual actuator:

$$B_{\text{Standard Arm}} = \left[B_{\text{Motor}} \;\; B_{\text{Servoblock}} \;\; B_{\text{Push Pull}} \right] \quad (16)$$

Now the column vector corresponding to each actuator are developed:

Thrusters:

- Thrust $T = \mu m$
- Drag Torque: $Q_d = \kappa m$
- Thrust Torque: $Q = lT = l\mu m$

$$B_{\text{Motor}} = B_{\text{Motor}_{\text{Thrust}}} + B_{\text{Motor}_{\text{Drag}}} + B_{\text{Motor}_{\text{Thrust Torque}}} = \begin{bmatrix} 0 \\ 0 \\ 0 \\ \mu \end{bmatrix} + \begin{bmatrix} 0 \\ 0 \\ \pm\kappa \\ 0 \end{bmatrix} + \begin{bmatrix} -l\mu \\ 0 \\ 0 \\ 0 \end{bmatrix} = \begin{bmatrix} -l\mu \\ 0 \\ \pm\kappa \\ \mu \end{bmatrix} \quad (17)$$

Servoblock:

- Thrust vectoring Torque: $HT_0\eta$ and $lT_0\eta$
- Gyroscopic Torque: $J\Omega\dot{\eta} \approx J\Omega\frac{\eta}{t_r}$

$$B_{\text{Servoblock}} = B_{\text{Servoblock}_{\text{Thrust}}} + B_{\text{Servoblock}_{\text{Gyro}}} = \begin{bmatrix} 0 \\ HT_0 \\ lT_0 \\ 0 \end{bmatrix} + \begin{bmatrix} \frac{-J\Omega}{t_r} \\ 0 \\ 0 \\ 0 \end{bmatrix} = \begin{bmatrix} \frac{-J\Omega}{t_r} \\ HT_0 \\ lT_0 \\ 0 \end{bmatrix} \quad (18)$$

Push Pull:

- Thrust vectoring: $HT_0\gamma$
- Gyroscopic Torque: $J\Omega\dot{\gamma} \approx J\Omega\frac{\gamma}{t_r}$

$$B_{\text{Push Pull}} = B_{\text{Push Pull}_{\text{Thrust}}} + B_{\text{Push Pull}_{\text{Gyro}}} = \begin{bmatrix} HT_0 \\ 0 \\ 0 \\ 0 \end{bmatrix} + \begin{bmatrix} 0 \\ \frac{J\Omega}{t_r} \\ 0 \\ 0 \end{bmatrix} = \begin{bmatrix} HT_0 \\ \frac{J\Omega}{t_r} \\ 0 \\ 0 \end{bmatrix} \quad (19)$$

All these three actuators in the standard arm put together yield the control effectiveness matrix of the standard arm $B_{\text{Standard Arm}}$.

$$B_{\text{Standard Arm}} = \left[B_{\text{Motor}} \;\; B_{\text{Servoblock}} \;\; B_{\text{Push Pull}} \right] = \begin{bmatrix} -l\mu & \frac{-J\Omega}{t_r} & HT_0 \\ 0 & HT_0 & \frac{J\Omega}{t_r} \\ \pm\kappa & lT_0 & 0 \\ \mu & 0 & 0 \end{bmatrix} \quad (20)$$

With the submatrix B known for the standard arm, $B_{\text{Standard Arm}}$, obtaining the B matrix of all the arms is just a matter of rotating the axes. If $R_{\text{Standard 2 n}}$ is the rotation matrix from the standard arm to Arm n, then:

$$B_{\text{Arm n}} = R_{\text{Std2n}} B_{\text{Standard Arm}} \tag{21}$$

The last step is to introduce wether the propellers are turningclockwise or anticlockwise in the signs of κ and Ω and assembling all the submatrices B for each arm to form the final B matrix:

$$B = \left[B_{\text{Arm 1}} \; B_{\text{Arm 2}} \; B_{\text{Arm 3}} \; B_{\text{Arm 4}} \right] \tag{22}$$

The B matrix represents, then, a linear approximation to the forces and moment generated by each actuator command:

$$\mathbf{v} = \begin{bmatrix} M \\ N \\ L \\ T \end{bmatrix} \approx B\mathbf{u} = \begin{bmatrix} 0 & HT_0 & \frac{J\Omega}{t_r} & 0 & -HT_0 & \frac{J\Omega}{t_r} & -l\mu & \frac{J\Omega}{t_r} & HT_0 & l\mu & \frac{J\Omega}{t_r} & -HT_0 \\ l\mu & \frac{J\Omega}{t_r} & -HT_0 & -l\mu & \frac{J\Omega}{t_r} & HT_0 & 0 & HT_0 & -\frac{J\Omega}{t_r} & 0 & -HT_0 & -\frac{J\Omega}{t_r} \\ -\kappa & lT_0 & 0 & \kappa & lT_0 & 0 & \kappa & lT_0 & 0 & -\kappa & lT_0 & 0 \\ \mu & 0 & 0 & \mu & 0 & 0 & \mu & 0 & 0 & \mu & 0 & 0 \end{bmatrix} \begin{bmatrix} m_1 \\ \eta_1 \\ \gamma_1 \\ m_2 \\ \eta_2 \\ \gamma_2 \\ m_3 \\ \eta_3 \\ \gamma_3 \\ m_4 \\ \eta_4 \\ \gamma_4 \end{bmatrix} \tag{23}$$

Note that the B matrix represents the relation between the inputs such as servo angle demands and the throttle and moments. Therefore, the units in the B matrix are not identical and this may cause some issues due to the different order of magnitudes embedded in the unit representation of the inputs. In order to avoid this problem, the B matrix is normalised, so that all the inputs range from -1 to 1 regardless of whether they are deflection angles or throttle positions. The new normalised B matrix will be represented by $\hat{B}$. To do so, a matrix E is defined whose diagonal term is given by the maximum absolute of the actuator limits, that is, $E_{ii} = \max(|\underline{u}_i|, |\bar{u}_i|)$. Then the normalised B matrix will be given by: $\hat{B} = BE$. Therefore all the inputs will be given by $\hat{\mathbf{u}} = E^{-1}\mathbf{u}$ which is normalised, i.e., $-1 \leq \hat{u}_i \leq 1$.

Allocator Design The control allocator problem can be posed as a quadratic minimisation problem: Find a matrix $\hat{B}^*$ such that,

$$\min_u \frac{1}{2}\hat{\mathbf{u}}^T W \hat{\mathbf{u}} \tag{24}$$

$$\text{subject to} \qquad \mathbf{v}_c - \hat{B}\hat{\mathbf{u}} = 0 \tag{25}$$

where $\hat{\mathbf{u}} = \hat{B}^*\mathbf{v}_c$. Note that an analytical solution of the optimal control allocation problem is given by the weighted pseudoinverse:

$$\hat{B}^* = W^{-1}\hat{B}^T\left(\hat{B}W^{-1}\hat{B}^T\right)^{-1} \tag{26}$$

As shown in Eq. 26 and the optimal solution of the allocation problem, the weight matrix W determines the characteristics of the optimal solution. Thus, the optimal allocation problem in this study can considered as a problem finding a appropriate weight matrix, W, such that they give a satisfactory blend of the different effectors.

Before determining the weight matrix, different control actuations must be understood. As expected, from a few tests and analysis, it is concluded that the gyroscopic action is fast and decays with time while the propulsive or motor action is rather slow but persistent in time. Figure 7 visualises the difference. As shown in Fig. 7, the normalised step response of a gyroscopic pitching moment and a propulsive pitching moment are shown together.

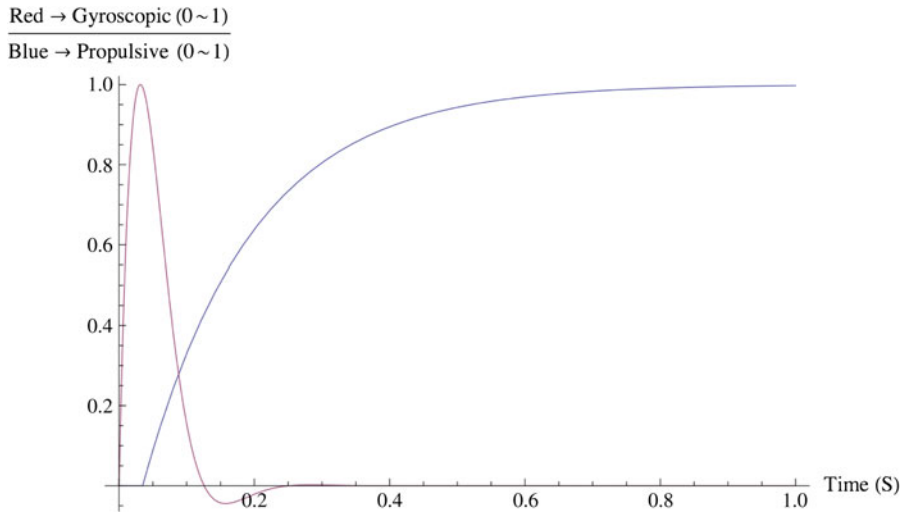

Fig. 7 Normalised pitching moment response generated by the motors following a differential step and the servo gyroscopic effects following a step at time 0. Note difference in time scales

In this paper, the weights of the W matrix are selected in a way that they blend both the gyroscopic effects and the motor action. The higher the element of an actuator is, the higher the cost it will have, and the more it will be minimised, i.e., the least used will be. To do this, a weight w_{motor} such that $0 < w_{\text{motor}} < 1$ was added in the elements corresponding to the motors and a weight $w_{\text{gyro}} = \frac{1-w_{\text{motor}}}{2}$ was added in the elements corresponding to the servos. So that for each arm all the weights were 1, i.e., $1 = w_{\text{gyro}} + w_{\text{gyro}} + w_{\text{motor}}$.Thus, the larger w_{motor} the smaller the use of the motors will be and the larger the use of the servos will be. Summing up, the weighting matrix is given by:

$$W = \begin{bmatrix} w_{\text{motor}} & & & & & & \\ & w_{\text{gyro}} & & & & 0 & \\ & & w_{\text{gyro}} & & & & \\ & & & w_{\text{motor}} & & & \\ & & & & w_{\text{gyro}} & & \\ & 0 & & & & \ddots & \\ & & & & & & w_{\text{gyro}} \end{bmatrix}$$

$$\text{where:} \qquad w_{\text{gyro}} = \frac{1 - w_{\text{motor}}}{2} \tag{27}$$

By selecting w_{motor} the relation between motor actuation and gyroscopic, or servo actuation, was altered. Thus, allowing to blend of the servo "kick" and the motor actuation to shape the response of the actuators. This mixing concept is illustrated in Fig. 8.

Several weights were tested by spanning w_{motor} from 0 to 1, and the response to a step at time 0 in the pitching moment was recorded and normalised. The result is shown in Fig. 9. From Fig. 9 it can be inferred that too large values of w_{motor} yield responses that have a significant overshoot, while small values of w_{motor} make the response visibly slower. Another issue to take into account is that, the larger the use of the servos, the larger is the likelihood of them being saturated.

As a trade-off between speed and excessive overshoot, it was concluded that a 15 % of overshoot would be desirable. To find which was the weight that gave 15 % of overshoot, an interpolation from the previous tested weights with its corresponding overshoots was carried out. The solution yielded that the value w_{motor} that makes the overshoot 15 % given by $w_{\text{motor}} = 0.994$.

In Fig. 10 the response to a step with the combination given by $w_{\text{motor}} = 0.994$ is shown. In Table 2 all the performance parameters are summarised and compared. It is clear that the response with allocator is faster than with differential thrusting. This faster response is also obvious from the bode plot of both effectors shown in Fig. 11, where the new actuator suite brings an order of magnitude improvement in bandwidth.

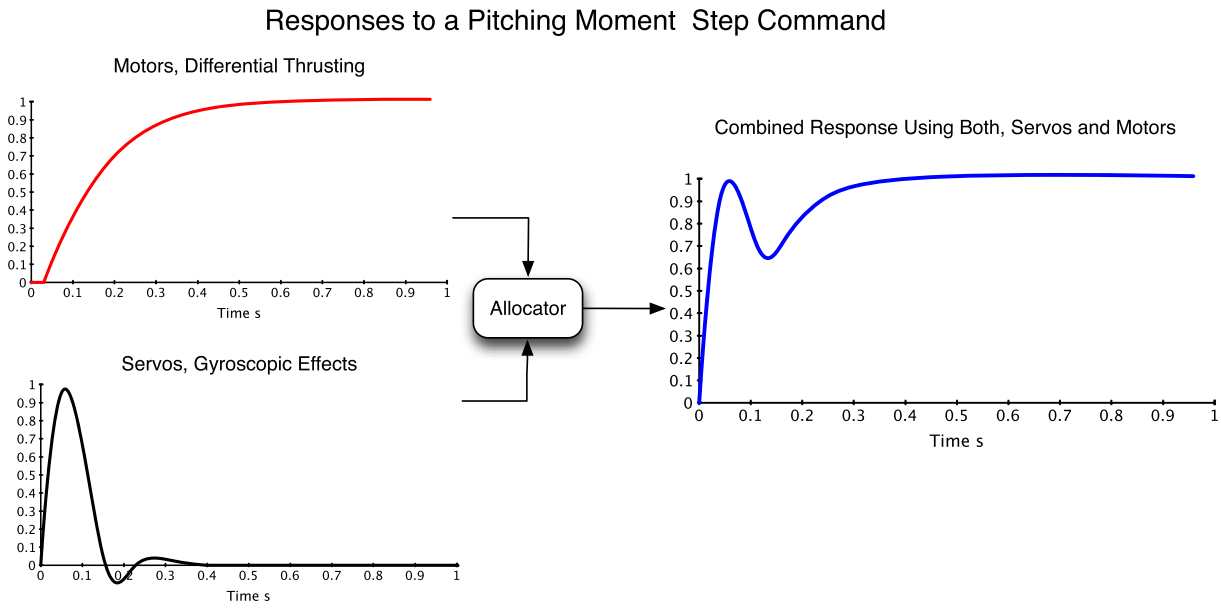

Fig. 8 Illustration of the concept of the control allocator as a "mixer" of the two kinds of effectors. Note that all the responses are normalised

4.2 Controller Tuning

The control law designed was a Proportional-Derivative, PD, loop for each axis independently, that took the readings and issued demands of torque to the control allocator. The approach followed to tune the controller gains was a mixture of model based tuning and testing with the real vehicle on a rig.

A simplified SISO model was produced for each axis with the structure shown in Fig. 12. From that model a transfer function was obtained and its characteristics on the frequency domain could be analysed. Thus, by visualising the frequency responses, an informative quantification of the quality parameters and a clear picture of the trends, performance indices and stability frontiers was obtained.

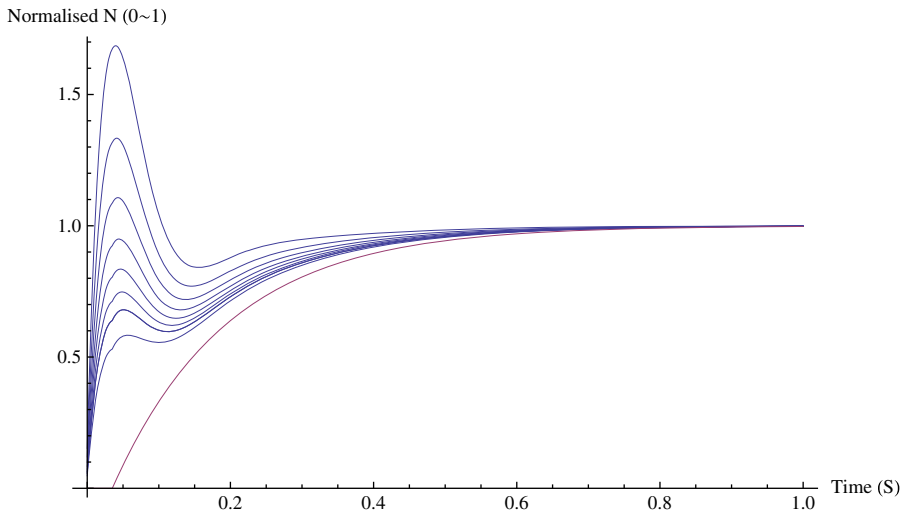

Fig. 9 Normalised pitching moment response generated by the allocator for different weights w_{motor} ranging from 0 to 1. Note the red line when $w_{\text{motor}} \approx 0$, thus, being basically executed by the motors alone

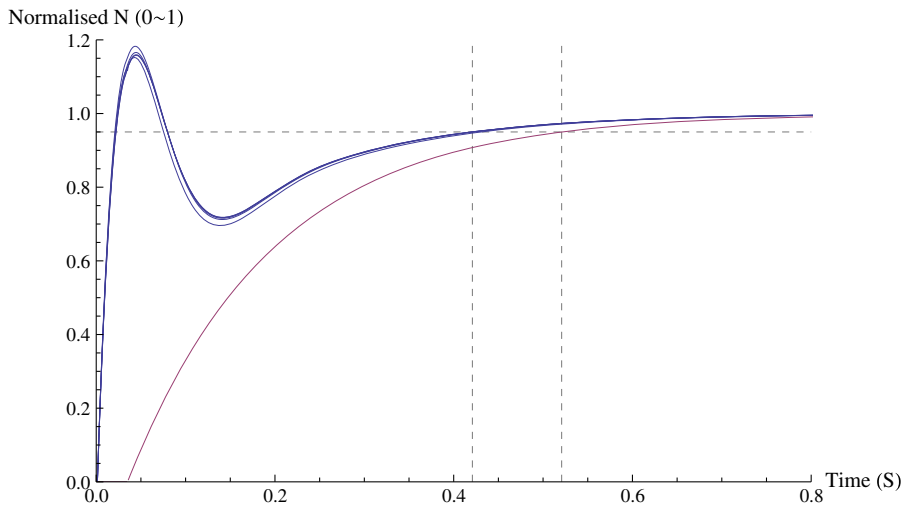

Fig. 10 Resulting allocator with $w_{\text{motor}} = 0.994$. *Blue lines* show the responses for several Pitching Moment (N) step commands from 0 to 1 Nm. The *red line* represents the response when $w_{\text{motor}} \approx 0$. Note the *dashed lines* showing the settling time (95 %) for the two actuator combinations

However, analytical models only are simplification of reality and so several potentially important effects are neglected. In this paper, those included actuator saturation (specially servomotors), processing and communication delays and neglected coupling dynamics because of the SISO approach. To avoid this, a combined strategy was devised. Essentially, the procedure was to find gains that gave desirable characteristics on the frequency domain and, then, testing them in the real vehicle on the rig to see its performance. Hence, by testing the gains of the vehicle, the real sensor measurements, processing and communication delays and the full dynamics were taken into consideration as well.

To easily manipulate the gains and see the immediate results, a graphical interface was constructed in Mathematica with two sliders, one for the K_P and one for the K_D. With this facility it was very easy to test and play with the gains, thus, resulting in a deeper understanding of the

Table 2 Comparison of the speed of the response of both control actions

Allocator	Rise T. t_r (s)	Settling T. t_s (s)	Bandwidth. $(\frac{rad}{s})$
Combination, $w_{\text{motor}} = 0.994$	0.024	0.42	100
Motors only $w_{\text{motor}} = 0$	0.52	0.52	6.1
Improvement	**95 %**	**20 %**	**≈1600 %**

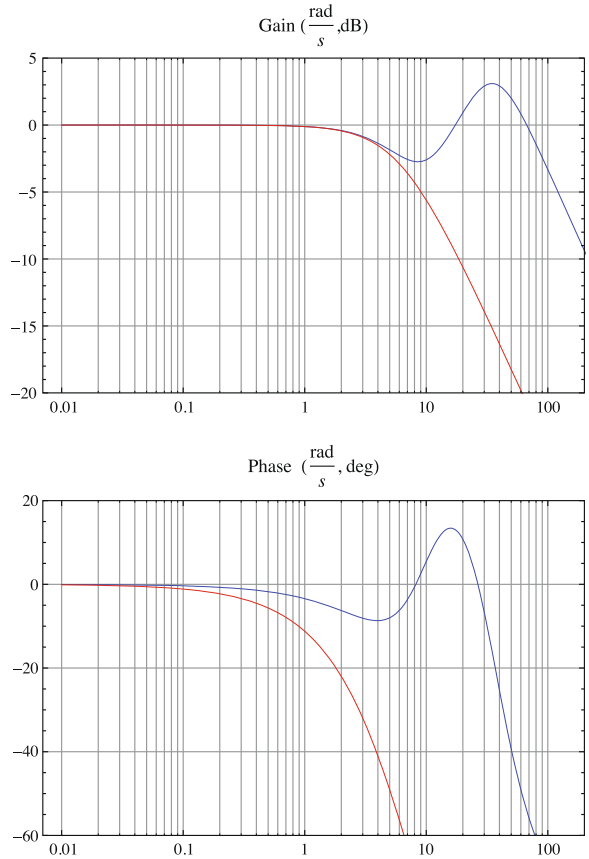

Fig. 11 Frequency response of the different sets of effectors. *Blue* using weighted pseudoinvrese allocator and *red* using differential thrusting approach

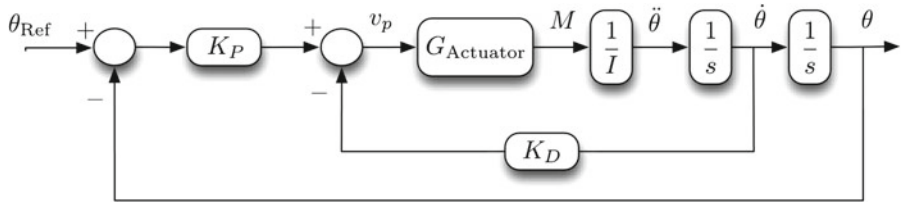

Fig. 12 Structure of the PD controller for the pitching dynamics

effects and trends. While, at the same time, it provided a quantified measure of the quality of the response in terms of the Peaks M_T and M_S. And, more relevantly, it raised awareness on the effects of possible changes in the gains showing the trends that each gain introduced on the response. This was fundamental because in provided a much deeper insight on the suitability of each combination of gains than what could have been achieved by a conventional trial and error tuning on the rig.

To test the controller on the vehicle, it was attached to a ball joint in a way that it constrained only the position, thus, allowing the 3 angular motions, Roll, Pitch and Yaw to be free and constraining only the translational motion. The setup of the test rig is illustrated in Fig. 13. The most relevant inconvenience of this setup is that there exists an offset between the ball and the vehicle's centre of gravity. This exerted an inverted-pendulum-like destabilising moment to the vehicle. Hence, it made vehicle more unstable than when flying.

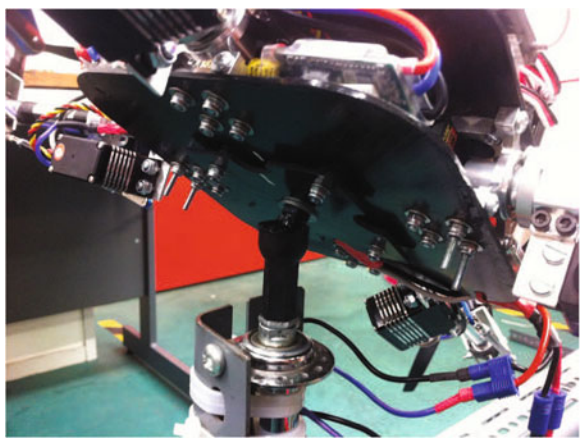

Fig. 13 Detail of the ball joint rig

Finally a design was found that for pitch and roll with the following gains: $K_P = 2.5$ and $K_D = 0.38$. The characteristic parameters of the frequency response are:

$$M_T = 1.90\text{dB} \qquad M_S = 3.79\text{dB}$$
$$\omega_c = 3.83\frac{\text{rad}}{s}\frac{\text{d}S}{\text{d}\omega}_{\text{Low Freq}} = -20\frac{\text{dB}}{\text{dec}} \tag{28}$$

and the stability margins are:

$$GM = 23.6\text{dB} \qquad PM = 78.62^\circ \tag{29}$$

5 Test and Design Validation

5.1 Test and Validation on the rig

The validation of the mathematical model is represented in [3] and it is shown that the overall the simulation model qualitatively follows the trends of the real vehicle with fidelity. In order to validate the proposed concept and tune the control system, a set of typical tests on the ball joint rig has been carried out. The sequence followed is described below.

1) Holding the vehicle, a slow throttle ramp command is sent to the vehicle. Once the nominal rpm have been obtained, the vehicle is released to verify **stability**.
2) A series of perturbations was introduced to test the controller for **disturbance rejection**. This was done by pushing the vehicle in each of axis with a foam handle. A sample recovery sequence is depicted in Fig. 14.
3) Finally, the controller was tested for **reference tracking**. The time histories for a sample test are presented for each axis see, Fig. 15 for Roll, Fig. 16 for Pitch and Fig. 17 for Yaw.

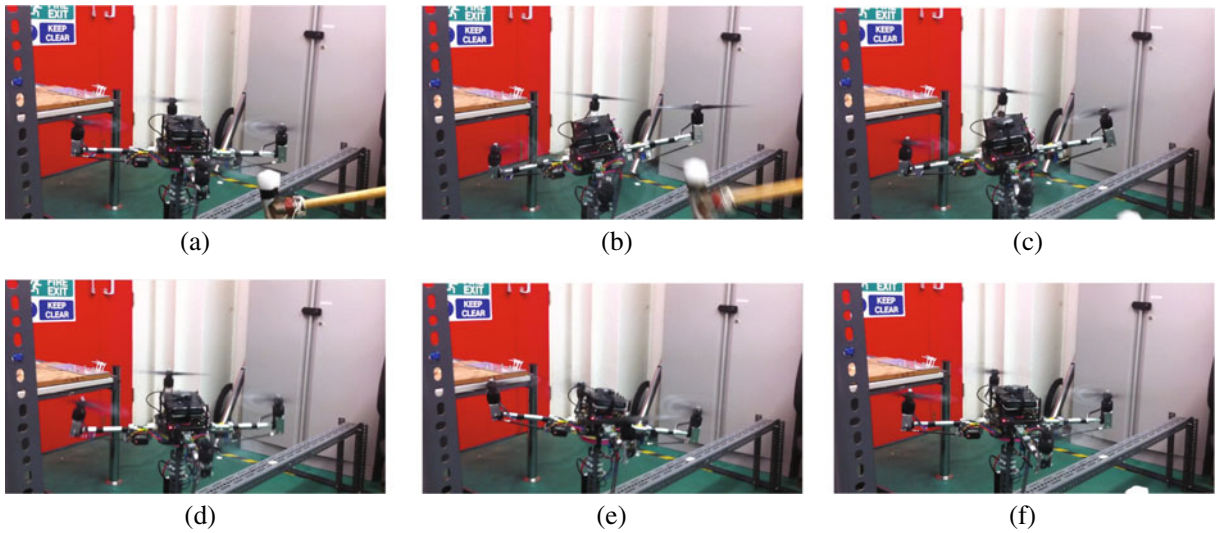

Fig. 14 Vehicle recovery after a disturbance test

As shown in Figs. 15, 16 and Fig. 17, the proposed control system works reasonably well, but it shows a considerable overshoot and delay. However, a similar tendency was observed in the numerical simulation results once the ball rig effects were introduced [3]. With the ball rig effects removed, this tendency diminished significantly, therefore, it is likely that the overshooting is caused by the inverted-pendulum-like moments introduced by the ball.

5.2 Flight Test and Validation

Once the control was tuned and satisfactory performance was achieved, the fist flight was attempted. The vehicle took-off, see Fig. 18, hovered for about minute and then landed. Relevant flight variables of interest were recorded and are shown in this Fig. 19. The data recorded is shown in a series of figures, the data has been organised by axes according to each control loop. For

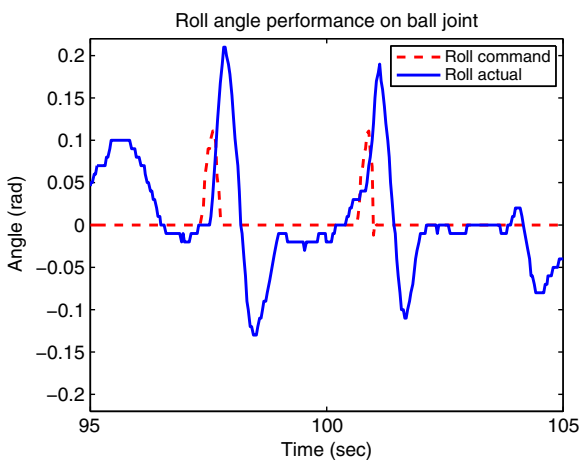

Fig. 15 Roll angle command tracking at ball joint rig

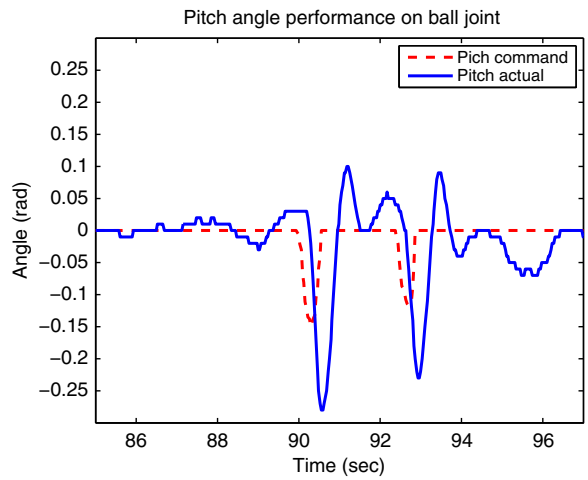

Fig. 16 Pitch angle command tracking at ball joint rig

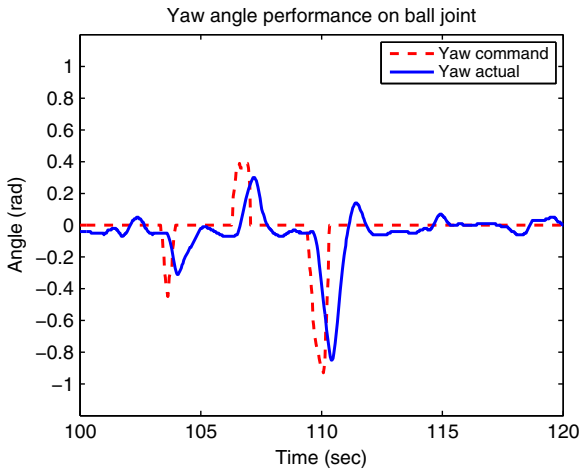

Fig. 17 Yaw angle command tracking at ball joint rig

each axis, the variables shown are the angle commanded, the actual angle, the angular rate and the total moment resulting from the control law. To evaluate the performance of the controller. The throttle history was also monitored, ranging from −50 % to 50 %, −50 % meaning zero throttle and 50 % meaning full throttle.

The first flight was the last stage of the vehicle construction, hence, it was intended to be just a validation of the sizing of the vehicle and the stability of the control system. Therefore, no quantitative conclusions are extracted from it. Further flight testing should imply quantitative comparisons based on systematic testing to analyse relevant variables in order to further validate the simulation model and to improve the control system. However, from it, it can be concluded that the vehicle is stable and able to maintain its attitude, all its systems performed as expected and it had plenty of control authority.

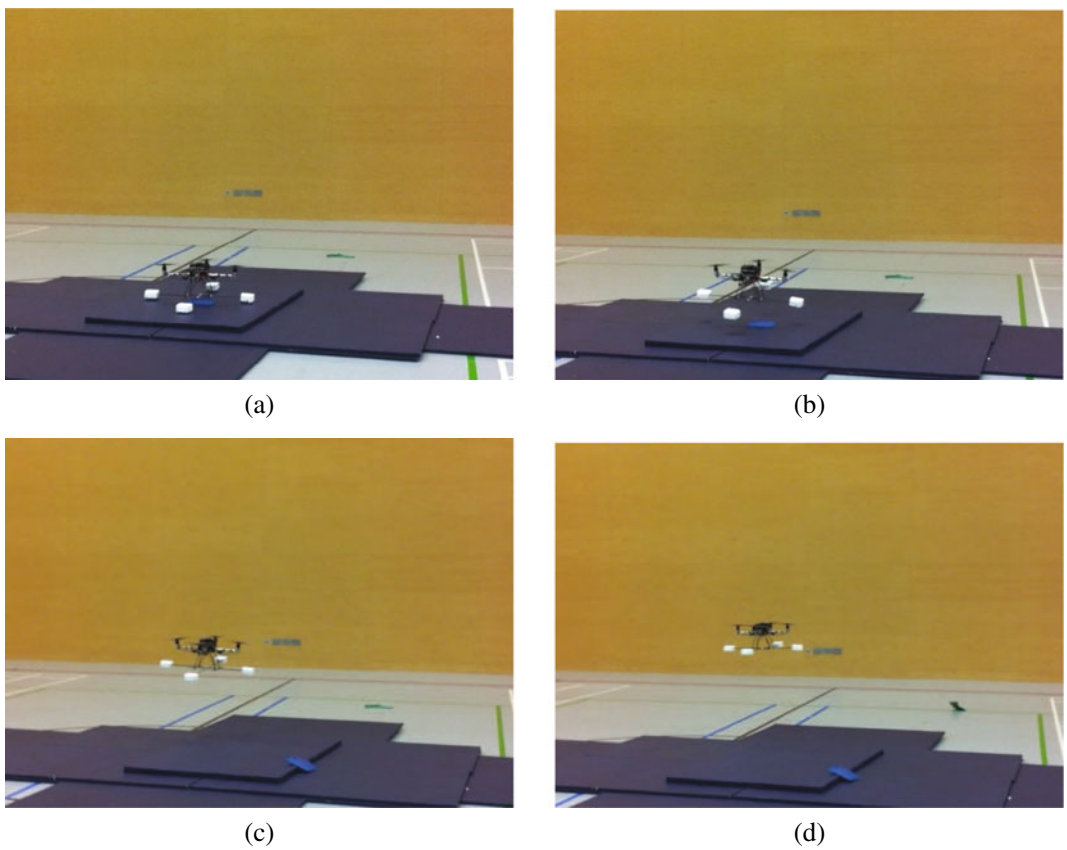

Fig. 18 First Flight: takeoff

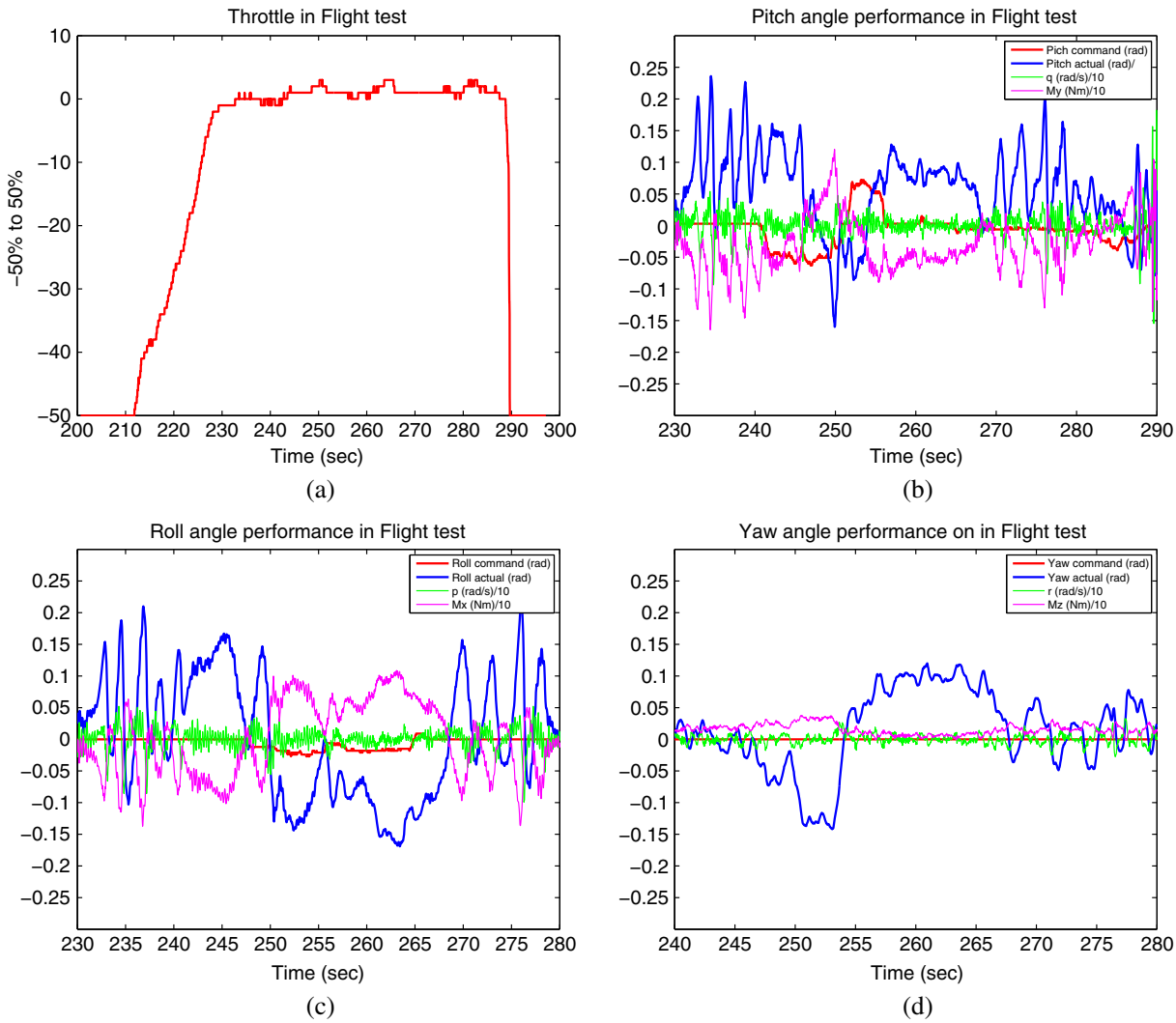

Fig. 19 Data recorded during the first flight. Please not the $\frac{1}{10}$ scaling where stated in the legend

6 Analysis and Discussion

There are two main objectives in this study: the first one is to improve the performance, and the second one to enhance fault tolerance capability over that of a conventional quadrotor. In this section, the performance improvement is verified by comparing the response to an identical vehicle with the conventional actuation. Then, the fault tolerant capabilities are verified experimentally by switching off the motors in two arms and checking for stability and disturbance rejection on the rig.

6.1 Performance Analysis

To put the performance into perspective, it is necessary to compare it against a baseline. The aim of this study is to develop an innovative actuated vehicle, hence, the logical step is to compare its equivalent conventionally actuated vehicle. Thus, a model of the pitching/rolling dynamics of the same quadrotor dynamics was developed, but, this time the function G_{Acuators} was equivalent to a differential thrust dynamics, i.e., G_{Motor}. In order to make the systems comparable, the controller of this conventional quadrotor was tuned so that its

dominant poles laid at the same position of those of the gyroscopically actuated vehicle.

Let's start the comparison with the closed loop function peaks:

$$M_T = 1.90\text{dB} \qquad M_S = 3.79\text{dB} \tag{30}$$

$$M_{T_{\text{motors}}} = 2.07\text{dB} \qquad M_{S_{\text{motor}}} = 5.76\text{dec} \tag{31}$$

The target for these peaks are $M_T < 2\text{dB}$ and $M_S < 6\text{dB}$. Both peaks are lower using the new actuator suite than in the conventionally actuated quadrotor. This means that the stability and robustness of the new system has higher safeguards than with the conventional quadrotor. In which the limits imposed are only met in the case of M_S and they're violated in the case of M_T. This is better seen in the Stability Margins:

$$GM = 23.6\text{dB} \qquad PM = 78.62^\circ \tag{32}$$

$$GM_{\text{motors}} = 4.71\text{dB} \qquad PM_{\text{motors}} = 34.45 \tag{33}$$

The conventional quadrotor, has a very narrow gain margin, consequence of the violation limit of M_T. And, the phase margin is almost half that of the new design. Thus, it can be concluded that an overall better quality of the response of the new strategy's actuated quadrotor and a higher confidence level about its stability has been achieved. This is because the speed in the actuation system has been increased in the new strategy improving the slow motor dynamics. To compare the response in terms of speed, the bandwidth of both systems is compared:

$$\omega_c = 3.83\frac{\text{rad}}{s} \qquad \omega_{c_{\text{motor}}} = 2.68\frac{\text{rad}}{s} \tag{34}$$

The speed of the new vehicle is higher with the new strategy, consequence of the faster actuation. However, this is not the full potential of this concept it can be shown that a higher gain design exists that provide an increase on an order of magnitude in the control bandwith. However, this high gain design is not feasible because the limitation imposed by the servomotor deflection saturation. Preliminary estimations have shown that a redesign of the rotors to increase its inertia that with an overall vehicle weight overhead below 10 % of the total weight, can solve this issue, because if the rotor inertia is increased, smaller deflections are needed to produce the same torques. This remains

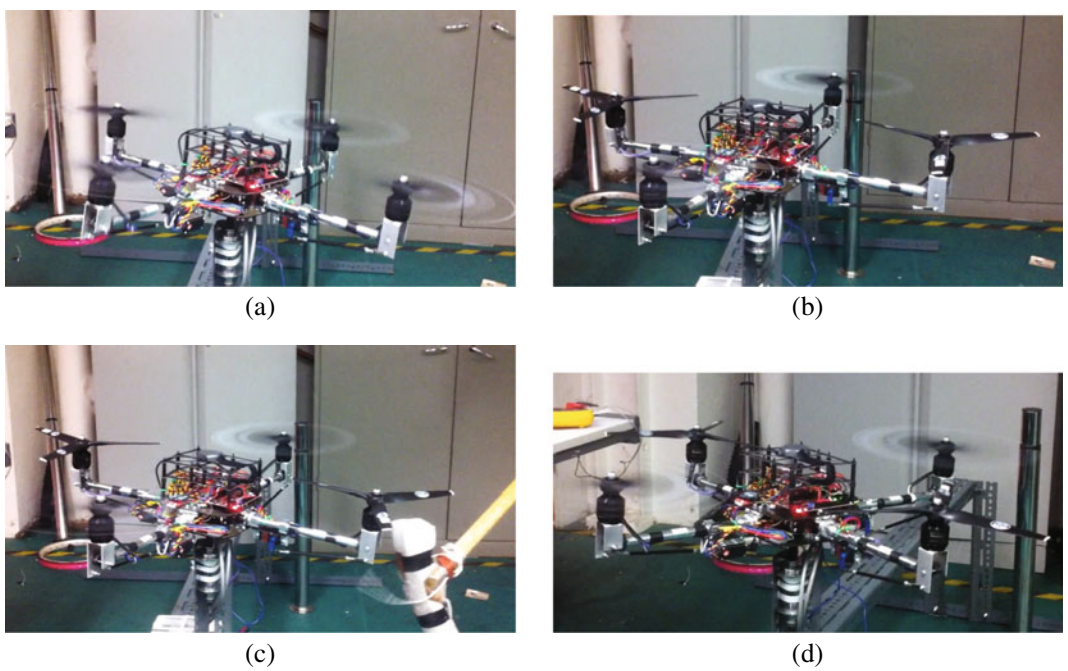

Fig. 20 Sequence of the two rotor failure test, note the stick in frame c to generate perturbations

an open area for future work and a combined inertial and aerodynamical design should be carefully looked at should a more advanced prototype be developed, because, if proven successful, it could yield an order of magnitude leap in performance.

6.2 Fault Tolerance

This actuator suite was also meant to increase the fault tolerance of the system increasing the number of individual actuator failures that don't generate a full destabilisation of the system. To explore these features the vehicle was tested against a two arm failure event. A new control allocator was designed by zeroing the columns corresponding to those actuators. Then, in the ball joint rig the vehicle was tested adding perturbations to check its stability. A sequence of these tests is shown in Fig. 20, where the vehicle is hovering on the rig, then two rotors are switched off and some perturbations are generated to check its performance. Of course, this is not a formal proof of all the capabilities that this strategy could yield, but rather a quick demonstration that this aspect can be a fruitful area for exploration in future work.

7 Conclusions

In this paper, a new innovative actuation strategy for multi rotors has been devised. In order to prove the proposed concept, a dual axis tilting UAV is designed and prototyped. Moreover, a control scheme based on the classical control theory and optimal control allocation is developed after mathematically obtaining a reasonable fidelity model of the vehicle. A series of tests on a ball joint rig and flight tests have been undertaken to validate the proposed concept and the designed control system. Comparing to a conventional actuation strategy in a quadrotor, i.e., based on varying propeller rpm, it is evidenced that the new actuation strategy could significantly increase the speed, performance of the actuator suite, and reliability of the quadrotor UAV. The actuators, have shown an order of magnitude increase in speed with the current design and the new strategy has also shown to be tolerant to actuator faults. However, in order to validate the proposed strategy more rigorously, further tests and analysis of the performance based on collected data are required.

Appendix

The gyrosocopic reactions of the standard arm are given by:

$$ {}^{1}\mathbf{M}_{\mathrm{Gyro}} = \mathbf{R}_{3\mathrm{to}1}(-{}^{3}\mathbf{M}) = \begin{bmatrix} {}^{1}\mathbf{M}_{\mathrm{Gyro}_X} \\ {}^{1}\mathbf{M}_{\mathrm{Gyro}_Y} \\ {}^{1}\mathbf{M}_{\mathrm{Gyro}_Z} \end{bmatrix} \tag{35} $$

where, after some tedious algebra:

$$
\begin{aligned}
{}^{1}\mathbf{M}_{\mathrm{Gyro}_X} = \frac{1}{4}\big(&-2I_{xx}qr + I_{yy}qr + I_{zz}qr + 3I_{yy}\cos(2\gamma)qr - 3I_{zz}\cos(2\gamma)qr - 4I_{zz}\sin(\gamma)\Omega r + 2I_{yy}\dot{\eta}r + 2I_{zz}\dot{\eta}r \\
&+ 2I_{yy}\cos(2\gamma)\dot{\eta}r - 2I_{zz}\cos(2\gamma)\dot{\eta}r - 2I_{xx}\dot{p} - I_{yy}\dot{p} - I_{zz}\dot{p} + I_{yy}\cos(2\gamma)\dot{p} - I_{zz}\cos(2\gamma)\dot{p} \\
&- 2I_{yy}p\sin(2\gamma)\dot{\gamma} + 2I_{zz}p\sin(2\gamma)\dot{\gamma} - \sin(2\eta)(4(I_{xx} - I_{yy})p\sin(\gamma)\Omega + 2(I_{yy} - I_{zz})r\sin(2\gamma)\dot{\gamma} \\
&- (2I_{xx} - I_{yy} - I_{zz})(\dot{r} + p(q + 2\dot{\eta})) - (I_{yy} - I_{zz})\cos(2\gamma)(\dot{r} + p(q + 2\dot{\eta}))) \\
&- \cos(2\eta)(4(I_{xx} - I_{yy})r\sin(\gamma)\Omega + 2(I_{zz} - I_{yy})p\sin(2\gamma)\dot{\gamma} + (2I_{xx} - I_{yy} - I_{zz})(\dot{p} - r(q + 2\dot{\eta})) \\
&+ (I_{yy} - I_{zz})\cos(2\gamma)(\dot{p} - r(q + 2\dot{\eta}))) - 2\cos(\eta)(2(I_{xx} - I_{yy} + I_{zz})\cos(\gamma)\Omega(q + \dot{\eta}) \\
&+ (I_{yy} - I_{zz})\sin(2\gamma)(q - r + \dot{\eta})(q + r + \dot{\eta}) + 2I_{xx}\ddot{\gamma}) \\
&- 2\sin(\eta)(-2(-I_{xx} + I_{yy} + I_{zz})\sin(\gamma)\Omega\dot{\gamma} - 2I_{xx}(q + \dot{\eta})\dot{\gamma} + 2(I_{yy} - I_{zz})\cos(2\gamma)(q + \dot{\eta})\dot{\gamma} \\
&+ 2I_{zz}\cos(\gamma)\dot{\Omega} - (I_{yy} - I_{zz})\sin(2\gamma)(pr - \dot{q} - \ddot{\eta}))\big)
\end{aligned}
$$

$$
\begin{aligned}
{}^{1}\mathbf{M}_{\mathrm{Gyro}_Y} = \frac{1}{4}\big(& -2I_{xx}\sin(2\eta)p^2 + I_{yy}\sin(2\eta)p^2 + I_{zz}\sin(2\eta)p^2 - 4I_{xx}\cos(2\eta)rp + 2I_{yy}\cos(2\eta)rp \\
& + 2I_{zz}\cos(2\eta)rp - 4I_{xx}\sin(\eta)\dot{\gamma}\,p + 2I_{xx}r^2\sin(2\eta) - I_{yy}r^2\sin(2\eta) - I_{zz}r^2\sin(2\eta) - 2I_{yy}\dot{q} - 2I_{zz}\dot{q} \\
& - 4I_{xx}\cos(\eta)r\dot{\gamma} - 4(I_{xx} - I_{yy} - I_{zz})\cos(\gamma)\Omega(\cos(\eta)p - r\sin(\eta) + \dot{\gamma}) \\
& + 2(I_{yy} - I_{zz})\sin(2\gamma)(-\sin(\eta)(qr + \dot{p}) + \cos(\eta)(pq - \dot{r}) + 2\dot{\gamma}(q + \dot{\eta})) + 4I_{zz}\sin(\gamma)\dot{\Omega} - 2I_{yy}\ddot{\eta} \\
& - 2I_{zz}\ddot{\eta} - 2(I_{yy} - I_{zz})\cos(2\gamma)(\dot{q} + (\cos(\eta)r + p\sin(\eta))(\cos(\eta)p - r\sin(\eta) + 2\dot{\gamma}) + \ddot{\eta})\big)
\end{aligned}
$$

$$
\begin{aligned}
{}^{1}\mathbf{M}_{\mathrm{Gyro}_Z} = \frac{1}{4}\big(& -2(I_{yy} - I_{zz})\sin(2\gamma)\sin(\eta)p^2 - (4(I_{yy} - I_{zz})\cos(2\gamma)\dot{\eta}\sin^2(\eta) + (2(-2I_{xx} + I_{yy} + I_{zz})\cos^2(\eta) \\
& - (I_{yy} - I_{zz})\cos(2\gamma)(\cos(2\eta) - 3))q - 4(I_{zz} + (I_{yy} - I_{xx})\cos(2\eta))\sin(\gamma)\Omega \\
& + 2(I_{yy} - I_{zz})\cos(\eta)\sin(2\gamma)(r + 2\sin(\eta)\dot{\gamma}) + 2(I_{yy} + I_{zz} + (-2I_{xx} + I_{yy} + I_{zz})\cos(2\eta))\dot{\eta})p \\
& - 2I_{xx}\dot{r} - I_{yy}\dot{r} - I_{zz}\dot{r} + I_{yy}\cos(2\gamma)\dot{r} - I_{zz}\cos(2\gamma)\dot{r} - 2I_{yy}r\sin(2\gamma)\dot{\gamma} \\
& + 2I_{zz}r\sin(2\gamma)\dot{\gamma} - \cos(2\eta)((-2I_{xx} + I_{yy} + I_{zz} + (I_{zz} - I_{yy})\cos(2\gamma))\dot{r} + 2(I_{yy} - I_{zz})r\sin(2\gamma)\dot{\gamma}) \\
& - \sin(2\eta)(4(I_{yy} - I_{xx})r\sin(\gamma)\Omega + (2I_{xx} - I_{yy} - I_{zz})(r(q + 2\dot{\eta}) - \dot{p}) \\
& + (I_{yy} - I_{zz})\cos(2\gamma)(r(q + 2\dot{\eta}) - \dot{p})) - 2\sin(\eta)(-(I_{yy} - I_{zz})\sin(2\gamma)(q + \dot{\eta})^2 \\
& - 2(I_{xx} - I_{yy} + I_{zz})\cos(\gamma)\Omega(q + \dot{\eta}) - 2I_{xx}\ddot{\gamma}) - 2\cos(\eta)(-2(-I_{xx} + I_{yy} + I_{zz})\sin(\gamma)\Omega\dot{\gamma} \\
& - 2I_{xx}(q + \dot{\eta})\dot{\gamma} + 2(I_{yy} - I_{zz})\cos(2\gamma)(q + \dot{\eta})\dot{\gamma} + 2I_{zz}\cos(\gamma)\dot{\Omega} + (I_{yy} - I_{zz})\sin(2\gamma)(\dot{q} + \ddot{\eta}))\big)
\end{aligned}
$$

References

1. Garcia, O., Sanchez, A., Escareño, J., Lozano, R.: Autonomous hovering of a noncyclic tiltrotor uav: modeling, control and implementation. In: Proceedings of the 17th World Congress The International Federation of Automatic Control. Seoul, Korea (2008)
2. Al-Rihani, Y.: Development of a dual axis tilt rotorcraft uav: design, prototyping and control. MSc Thesis, Cranfield University (2012)
3. Al-Rihani, Y., Gasco, P.S., Shin, H.-S., Savvaris, A.: Modelling and simulation of a novel dual axes tilt quadrotor uav. In: AIAA Modelling and Simulation Technologies Conference. Boston, USA (2013)
4. Cutler, M., Kemal Ure, N., Michini, B., How, J.P.: Comparison of fixed and variable pitch actuators for agile quadrotors. In: AIAA Guidance, Navigation, and Control Conference (GNC) (AIAA-2011-6406). http://acl.mit.edu/papers/GNC11_Cutler_uber.pdf (2011)
5. Gascó, P.S.: Development of a dual axis tilt rotorcraft uav: Modelling, simulation and control. Master's thesis, Cranfield University (2012)
6. Gress, G.R.: Using dual propellers as gyroscopes for tilt- prop hover control. In: Proc. AIAA Biennial Int. Powered Lift Conf. Exhibit. Williamsburg, VA (2002)
7. Gress, G.R.: Lift fans as gyroscopes for controlling compact vtol air vehicles: overview and development status of oblique active tilting. In: American Helicopter Society 63th Annual Forum. Virginia Beach, VA (2007)
8. Kendoul, F., Fantoni, I., Lozano, R.: Modeling and control of a small autonomous aircraft having two tilting rotors. In: 44th IEEE Conference on Decision and Control, 2005 and 2005 European Control Conference, CDC-ECC '05, pp. 8144–8149 (2005)
9. Moerder, Y-Y., Cooper, D.D., Lim, E.G, Shin, K.B.: A new approach to attitude stability and control for low airspeed vehicles. In: AIAA Guidance, Navigation and Control Conference and Exhibit. Providence, RI, United States 16–19 Aug. 2004
10. Lo, C.H., Shin, H.-S., Tsourdos, A., Kim, S.: Modeling and simulation of fault tolerant strategies for a quad rotor UAV. In: AIAA Modeling and Simulation Technologies Conference. American Institute of Aeronautics and Astronautics (2013). doi:10.2514/6.2012-4724
11. Mahony, R., Kumar, V., Corke, P.: Multirotor aerial vehicles: Modeling, estimation, and control of quadrotor. IEEE Robot. Autom. Mag. **19**(3):20–32 (2012)
12. Davies, R., Amiri, N., Ramirez-Serrano, A.: Modelling of opposed lateral and longitudinal tilting dual-fan unmanned aerial vehicle. In: 18th IFAC World Congress. Milano, Italy (2011)
13. ServoCity: http://www.servocity.com/ (2012)